nature neuroscience

SUPPLEMENTARY INFORMATION

https://doi.org/10.1038/s41593-018-0151-z

In the format provided by the authors and unedited.

Chronic CRH depletion from GABAergic, long-range projection neurons in the extended amygdala reduces dopamine release and increases anxiety

Nina Dedic[1,9], Claudia Kühne[1,9], Mira Jakovcevski[1], Jakob Hartmann[1,2], Andreas J. Genewsky[1], Karina S. Gomes[1,3], Elmira Anderzhanova[1], Max L. Pöhlmann[1], Simon Chang[1], Adam Kolarz[1], Annette M. Vogl[1], Julien Dine[1], Michael W. Metzger[1], Bianca Schmid[1], Rafael C. Almada[1], Kerry J. Ressler[2], Carsten T. Wotjak[1], Valery Grinevich[4], Alon Chen[1], Mathias V. Schmidt[1], Wolfgang Wurst[5,6,7], Damian Refojo[1,8] and Jan M. Deussing[1]*

[1]Department of Stress Neurobiology and Neurogenetics, Max Planck Institute of Psychiatry, Munich, Germany. [2]Department of Psychiatry, Harvard Medical School and McLean Hospital, Belmont, MA, USA. [3]Laboratory of Neuropsychopharmacology, Paulista State University, Araraquara, Brazil. [4]Schaller Research Group on Neuropeptides, German Cancer Research Center, Central Institute of Mental Health, University of Heidelberg, Heidelberg, Germany. [5]Institute of Developmental Genetics, Helmholtz Zentrum München, Munich, Germany. [6]Technische Universität München, Chair of Developmental Genetics, Munich, Germany. [7]German Center for Neurodegenerative Diseases (DZNE), Site Munich, Munich, Germany. [8]Instituto de Investigacion en Biomedicina de Buenos Aires (IBioBA)-CONICET-Partner Institute of the Max Planck Society, Buenos Aires, Argentina. 9These authors contributed equally: Nina Dedic, Claudia Kühne. *e-mail: deussing@psych.mpg.de

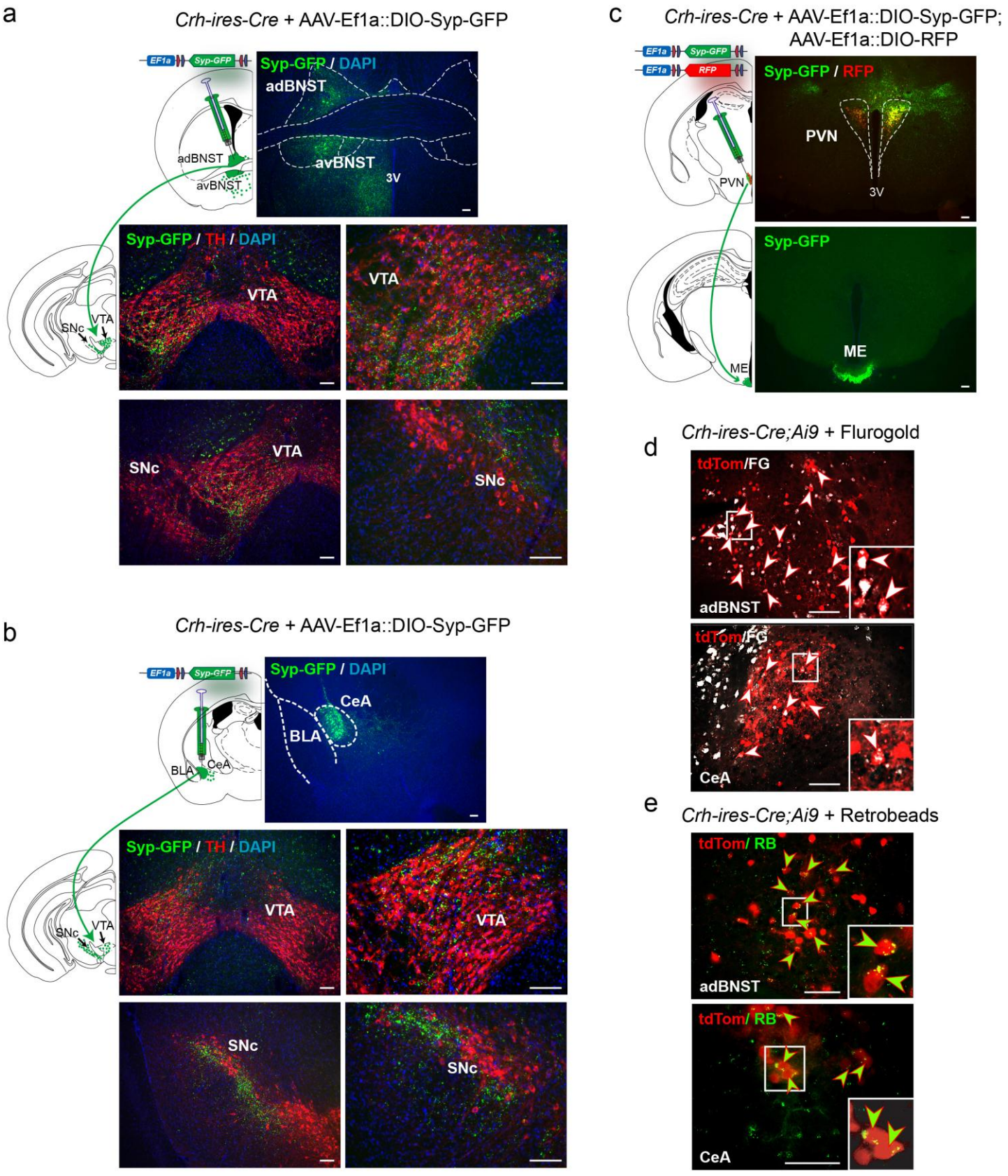

Supplementary Figure 1

CRH neurons in the aBNST and CeA directly project to the VTA and SNc.

Extension of Figure 1a,b. AAVs expressing a Cre-dependent Synaptophysin (Syp)-GFP fusion protein (AAV-Ef1a::DIO-Syp-GFP) were unilaterally injected into the aBNST or CeA of *Crh-ires-Cre* mice. Presynaptic Syp-GFP puncta are shown in green, immunostaining for tyrosine hydroxylase (TH), a dopaminergic marker, in red. The anterogradely labeled presynaptic terminals (Syp-GFP puncta) represent direct projection sites of aBNST and CeA CRH neurons. Prominent Syp-GFP labeling is observed throughout the VTA and SNc following AAV-Ef1a::DIO-Syp-GFP injections into the aBNST or CeA of *Crh-ires-Cre* mice. The density of Syp-GFP puncta in the VTA was higher in aBNST-injected compared to CeA-injected mice. The opposite was observed for the SNc, which received stronger input from CeA CRH neurons (**a,b**, bottom panels). Additional projection sites of aBNST and CeA CRH neurons, as well as of other CRH-expressing brain regions, are listed in Supplementary Table 1. Monosynaptic innervation of the VTA by CRH-expressing neurons of the CeA and aBNST has also been demonstrated by others[13,14,50]. (**c**) Accuracy of the tracing approach was verified by co-injecting AAV**-**Ef1a::DIO-Syp-GFP and AAV**-**Ef1a::DIO-RFP into the PVN. AAV**-**Ef1a::DIO-RFP helped to identify correctly targeted neurons at the injection site, since most Syp-GFP is transported to presynaptic terminals and thus often not visible in the cell soma. The highest Syp-GFP puncta density originating from the PVN was observed in the zona externa of the median eminence, the most prominent projection site of parvocellular CRH-positive PVN neurons. From there CRH is released into the hypophysial portal vasculature to initiate activation of the hypothalamic-pituitary-adrenal axis. (**d**) Projections from CeA and BNST to the VTA were further verified by retrograde tracing using Fluorogold (FG). FG injected to the VTA of *Crh-ires-Cre;Ai9* mice revealed a significant number of CRH/tdTomato positive neurons in the BNST and CeA co-labeled with FG. (**e**) Similarly, injection of retrobeads into the VTA of *Crh-ires-Cre;Ai9* mice resulted in CRH/tdTomato neurons co-labeled with retrobeads. All tracing experiments were independently replicated three times. Abbreviations: Anterior BNST (aBNST), anterior dorsal BNST (adBNST), anterior ventral BNST (avBNST), basolateral amygdala (BLA), central amygdala (CeA), median eminence (ME), paraventricular nucleus of the hypothalamus (PVN), substantia nigra pars compacta (SNc), substantia nigra pars reticularis (SNr), synaptophysin (Syp), third ventricle (3V), Ventral tegmental area (VTA). Scale bars represent 100 µm.

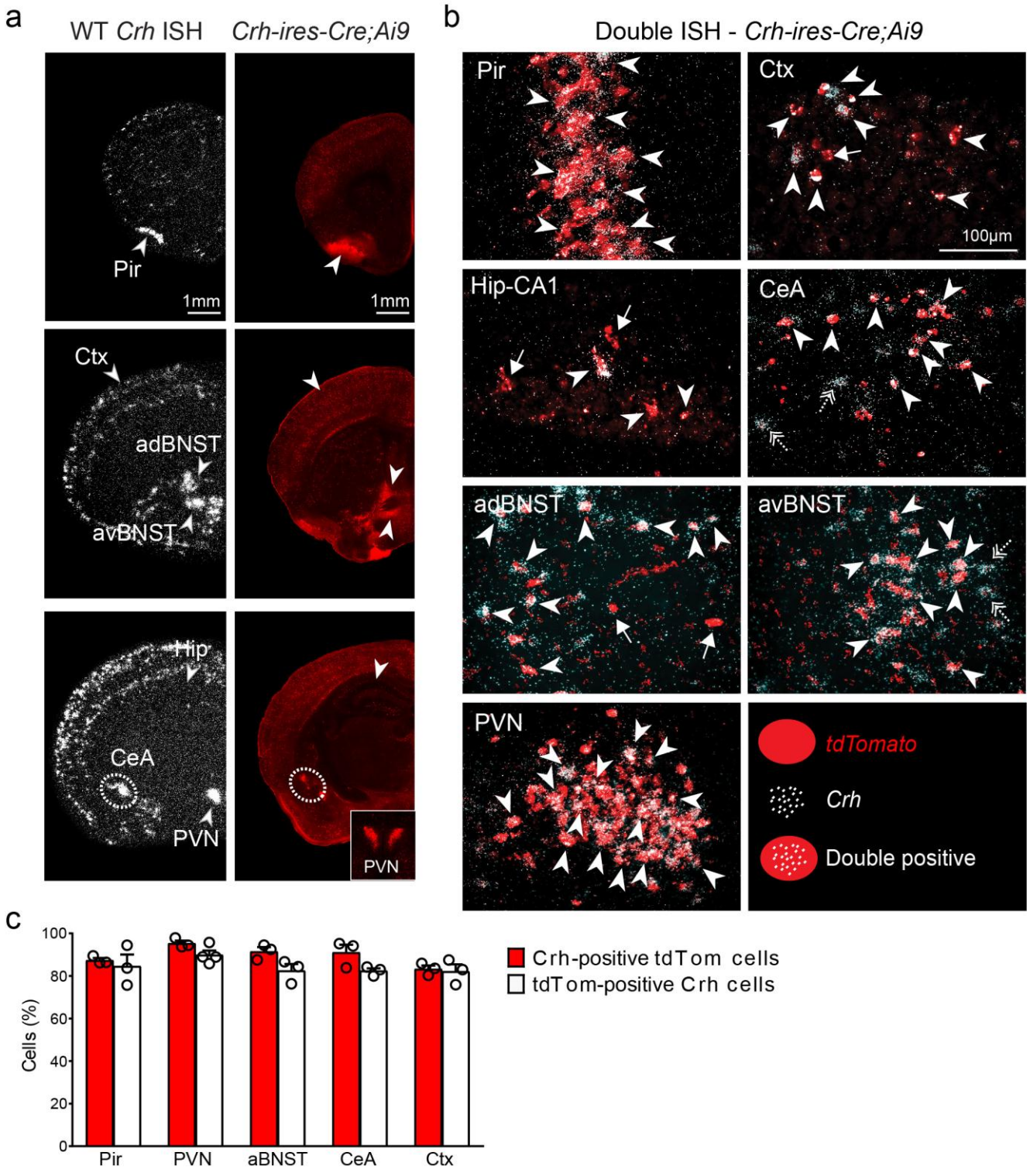

Supplementary Figure 2

***Crh-ires-Cre*-driven reporter expression faithfully reproduces native *Crh* expression patterns.**

Crh-ires-Cre mice were generated by inserting an *ires-Cre* expression cassette immediately after the translational STOP codon in the 3' UTR of the endogenous *Crh* gene[21]. As a result, *Cre* expression is

regulated by endogenous *Crh* promoter/enhancer elements, without compromising *Crh* expression. (**a**) Left row depicts the endogenous *Crh* mRNA expression pattern in adult wild-type mice (C57BL/6J) determined by ISH. Right row shows representative coronal sections of *Crh-ires-Cre* mice crossed with *Ai9* reporter mice (R26::*loxP-STOP-loxP-tdTomato*). tdTomato fluorescence (red) mirrors the native *Crh* mRNA expression pattern. Regions of interest are highlighted with arrowheads or dashed lines. Representative images of three independent experiments. (**b**) High specificity of Cre recombinase expression in CRH neurons was additionally confirmed by double ISHs against endogenous *Crh* (white) and *Crh-ires-Cre*-driven *tdTomato* (red). (**c**) Quantification of double positive cells in (b); n = 3 mice, 2-3 sections/mouse. Most tdTomato-expressing neurons co-expressed *Crh,* and likewise the majority of *Crh*-positive neurons also expressed *tdTomato* (arrowheads). Upon Cre/loxP recombination-mediated removal of the transcriptional STOP cassette from the R26CAG$^{::loxP\text{-}STOP\text{-}loxP\text{-}tdTomato}$ allele, tdTomato-reporter expression is driven by a CAG promoter and continuously detected in all neurons that have expressed CRH at any given time point within their lineage. Thus, *tdTomato*-positive neurons that lack *Crh* expression (arrows) could represent cells that expressed CRH during the course of development, but ceased to do so in adulthood. The presence of *Crh*-positive, but *tdTomato*-negative cells (dashed arrows), could be explained by lack of activity of the CAG promoter (that drives *tdTomato* expression) in those particular cells. Abbreviations: anterior dorsal BNST (adBNST), anterior ventral BNST (avBNST), central nucleus of the amygdala (CeA), cortex (Ctx), hippocampus (Hip), piriform cortex (Pir), paraventricular nucleus of the hypothalamus (PVN). Error bars represent s.e.m.

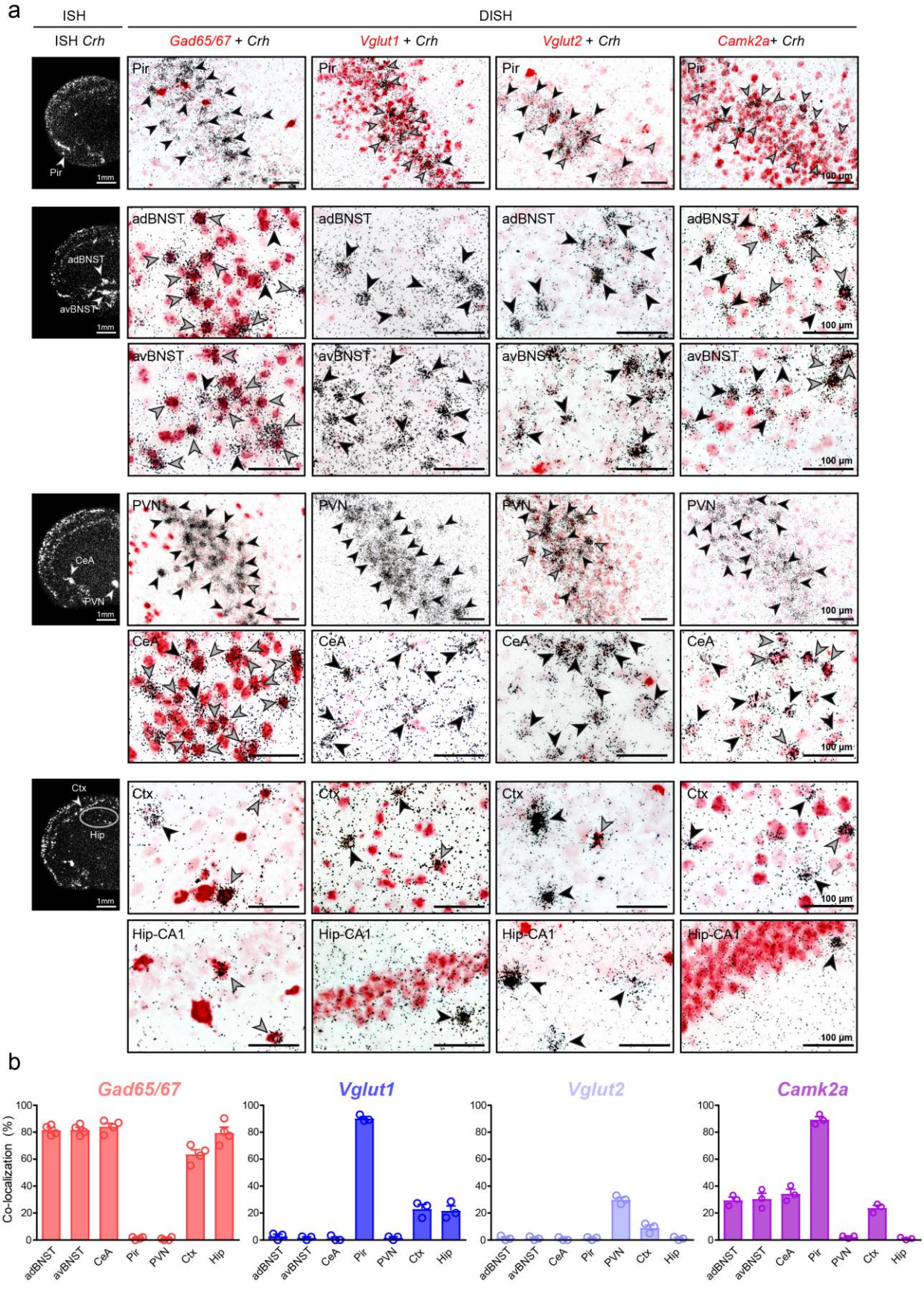
a
ISH
DISH
ISH Crh
Gad65/67 + Crh
Vglut1 + Crh
Vglut2 + Crh
Camk2a+ Crh
Pir
adBNST
avBNST
CeA
PVN
Ctx
Hip
Hip-CA1
1mm
100 μm
b
Gad65/67
Vglut1
Vglut2
Camk2a
Co-localization (%)
0
20
40
60
80
100
adBNST
avBNST
CeA
Pir
PVN
Ctx
Hip

Supplementary Figure 3

Neurochemical identity of *Crh*-expressing neurons in the mouse brain.

(**a**) The first left column depicts dark-field photomicrographs of the *Crh* mRNA expression pattern in brain sections of adult wild-type (C57BL/6) mice determined by ISH. Regions of interest are highlighted with arrowheads. Additional columns represent bright field photomicrographs of coronal wild-type brain sections showing double ISH of *Crh* mRNA (silver grains) together with different neuronal markers (red staining) including glutamic acid decarboxylase 65 and 67 (*Gad65/67*), vesicular glutamate transporters 1 and 2 (*Vglut1, Vglut2*) and calcium/calmodulin-dependent protein kinase 2 alpha (*Camk2a*). Black arrowheads indicate cells only expressing *Crh* (silver grains). Grey arrowheads indicate cells co-expressing *Crh* and the respective marker. All images are representatives of three independent experiments. (**b**) Quantifications of *Crh* co-expression with different neuronal markers (*Gad65/67* n = 4 mice; *Vglut1*, *Vglut2*, *Camk2a* n = 3 mice; adBNST, avBNST, CeA, Pir and Hip = 3 sections/mouse, Ctx = 5 sections/mouse). *Crh* neurons in the cortex and limbic regions such as the CeA, BNST and hippocampus are predominately GABAergic which coincides with previous reports[15,16,50]. Most CRH neurons in the piriform cortex are glutamatergic, and a few *Vglut1*- and *Vglut2*-expressing *Crh* neurons were also detected throughout the remaining cortical layers. Considering that *Camk2a* is primarily expressed in glutamatergic neurons suggests that CRH/CAMK2A-positive neurons in the piriform cortex and cortex most likely represent excitatory, *Vglut1* or *Vglut2*-positive cells. Contrastingly, *Crh/Camk2a* co-expressing neurons in the aBNST and CeA are GABAergic (see Main Text). Abbreviations: anterior dorsal BNST (adBNST), anterior ventral BNST (avBNST), central nucleus of the amygdala (CeA), cortical layers (CtxII/III, CtxV/VI), hippocampus (Hip), paraventricular nucleus of the hypothalamus (PVN), piriform cortex (Pir). Error bars represent s.e.m.

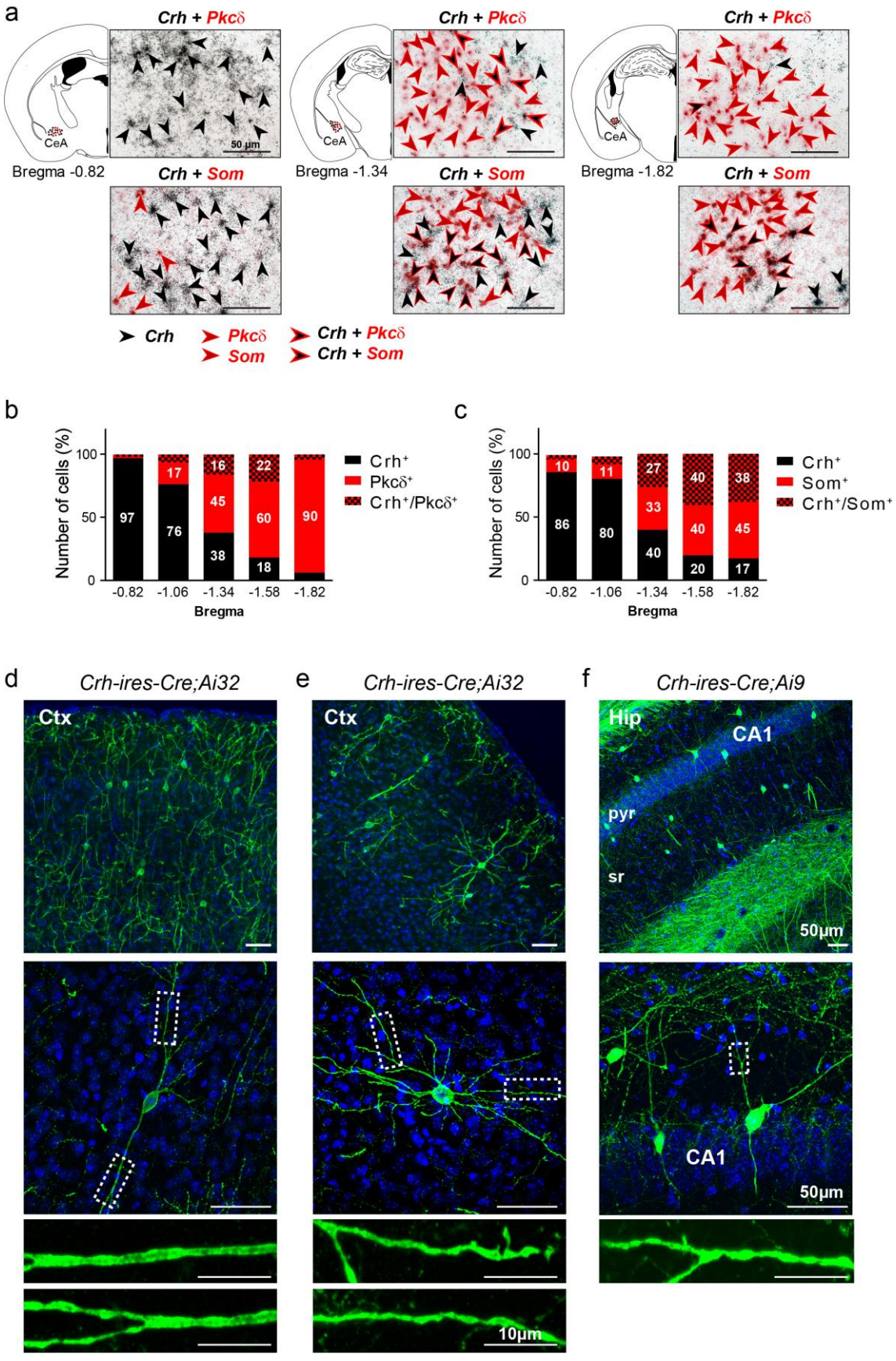
a
Crh + Pkcδ
Crh + Som
CeA
50 μm
Bregma -0.82
Bregma -1.34
Bregma -1.82
Crh
Pkcδ
Som
Crh + Pkcδ
Crh + Som
b
Number of cells (%)
Crh+
Pkcδ+
Crh+/Pkcδ+
97
17
76
16
45
38
22
60
18
90
-0.82
-1.06
-1.34
-1.58
-1.82
Bregma
c
Number of cells (%)
Crh+
Som+
Crh+/Som+
86
10
80
11
40
27
33
40
40
20
38
45
17
Bregma
d
Crh-ires-Cre;Ai32
Ctx
e
Crh-ires-Cre;Ai32
Ctx
10μm
f
Crh-ires-Cre;Ai9
Hip
CA1
pyr
sr
50μm
CA1
50μm

Supplementary Figure 4

Characterization of CRH neurons in the CeA and morphological assessment of cortical and hippocampal CRH neurons.

(**a**) Representative bright field photomicrographs of coronal wild-type brain sections covering the rostral to caudal extension of the CeA. Depicted are double ISHs of *Crh* mRNA (silver grains) together with CeA-specific markers (red staining) protein kinase C delta (*Pkcδ*) and somatostatin (*Som*). Black arrowheads indicate cells only expressing *Crh*. Red arrowheads indicate cells only expressing *Pkcδ* or *Som*, respectively. Double positive cells are indicated by black arrowheads enframed by a red line. In accordance with others[9,10], *Crh* neurons in the CeA appear to constitute a distinct GABAergic population as they show limited overlap with CeA markers *Pkcδ* or *Som.* (**b**) Quantification of *Crh* co-expression with *Pkcδ* at different CeA levels from bregma -0.82 to -1.82 (n = 3 mice from independent experiments). (**c**) Quantification of *Crh* co-expression with *Som* at different CeA levels from bregma -0.82 to -1.82 (n = 3 mice from independent experiments, 1-2 sections/mouse). (**d-f**) Overview of confocal images of the cortex (Ctx) and CA1 region of the hippocampus (Hip) in *Crh-ires-Cre;Ai32* (**d,e** top) and *Crh-ires-Cre;Ai9* (**f**, top) mice showing native ChR2-EYFP and tdTomato fluorescence (both in green) in CRH neurons. DAPI staining shown in blue. Higher power images illustrate that cortical (**d, e** middle) and hippocampal (**f**, middle) CRH neurons display bipolar and multipolar morphologies with aspiny dendrites (**d-f**, bottom) characteristic of GABAergic interneurons. Images in d-f are representatives from four independent experiments. Pyramidal cell layer (pyr), stratum radiatum (sr).

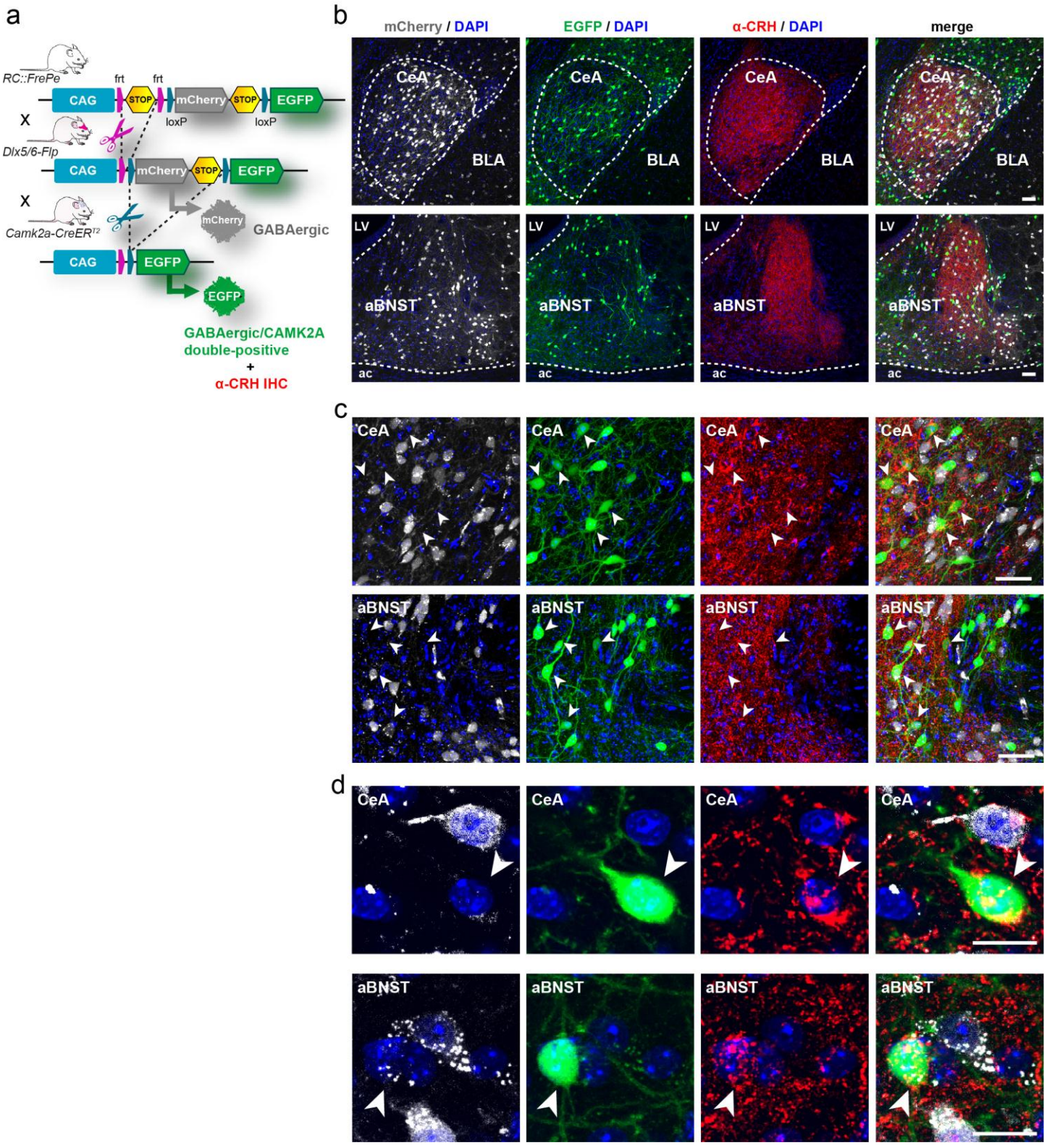

Supplementary Figure 5

Combining dual fate mapping with immunohistochemistry identifies triple-positive GABAergic/CAMK2A/CRH neurons in the anterior bed nucleus of the stria terminalis (aBNST) and central amygdala (CeA).

(**a**) Schematic illustration of the recombinase-based intersectional strategy used to genetically label double-positive GABAergic/CAMK2A neurons. *RC::FrePE* double-reporter mice[25,26] were initially crossed with *Dlx5/6-Flp* mice, leading to the excision of the *frt*-flanked *STOP* cassette and consequent expression of mCherry in *Dlx5/6*-positve (GABAergic) neurons. Subsequent crossing of *RC::FrePE;Dlx5/6* mice to *Camk2a-CreER^{T2}* mice leads to the excision of the *loxP*-flanked *mCherry-STOP* sequence, which results in the activation of EGFP expression within cells that have expressed both *Dlx5/6-Flp* and *Camk2a-CreER^{T2}* at any time and in any order within their lineage. Thus, EGFP fluorescence reports the presence of double-positive GABAergic/CAMK2A neurons, while mCherry labeling is observed in cells that only express *Dlx5/6-Flp* (exclusively GABAergic, non-CAMK2A-expressing neurons). Cre activity alone (solely CAMK2A-expressing neurons) is not reported. Immunohistochemistry against CRH was performed on coronal vibratome sections of *RC::FrePE;Dlx5/6;Camk2a-CreER^{T2}* mice. (**b**) Representative lower magnification confocal images showing native EGFP (green) and mCherry (gray) expression, as well as CRH immunostaining (red) in the aBNST and CeA of *RC::FrePE;Dlx5/6-Cre;Camk2a-CreER^{T2}* mice. The merged images demonstrate the presence of triple-positive GABAergic/CAMK2A/CRH neurons in the aBNST and CeA. The accuracy and specificity of this dual-fate mapping approach is demonstrated by the fact that only a few single GABAergic (mCherry, gray) and GABAergic/CAMK2A-positive (EGFP, green) neurons were detected in the basolateral amygdala (BLA), a structure that primarily contains excitatory glutamatergic neurons. (**c, d**) Representative higher magnification images of triple-positive GABAergic/CAMK2A/CRH neurons in the aBNST and CeA. Expectedly (and further proof of the accuracy and specificity of this dual-fate mapping approach) no co-localization is detected between the mutually exclusive mCherry- and EGFP-labeled neurons. All representative images were derived from three independent experiments. Scale bars in b-c = 50 µm; d = 20 µm.

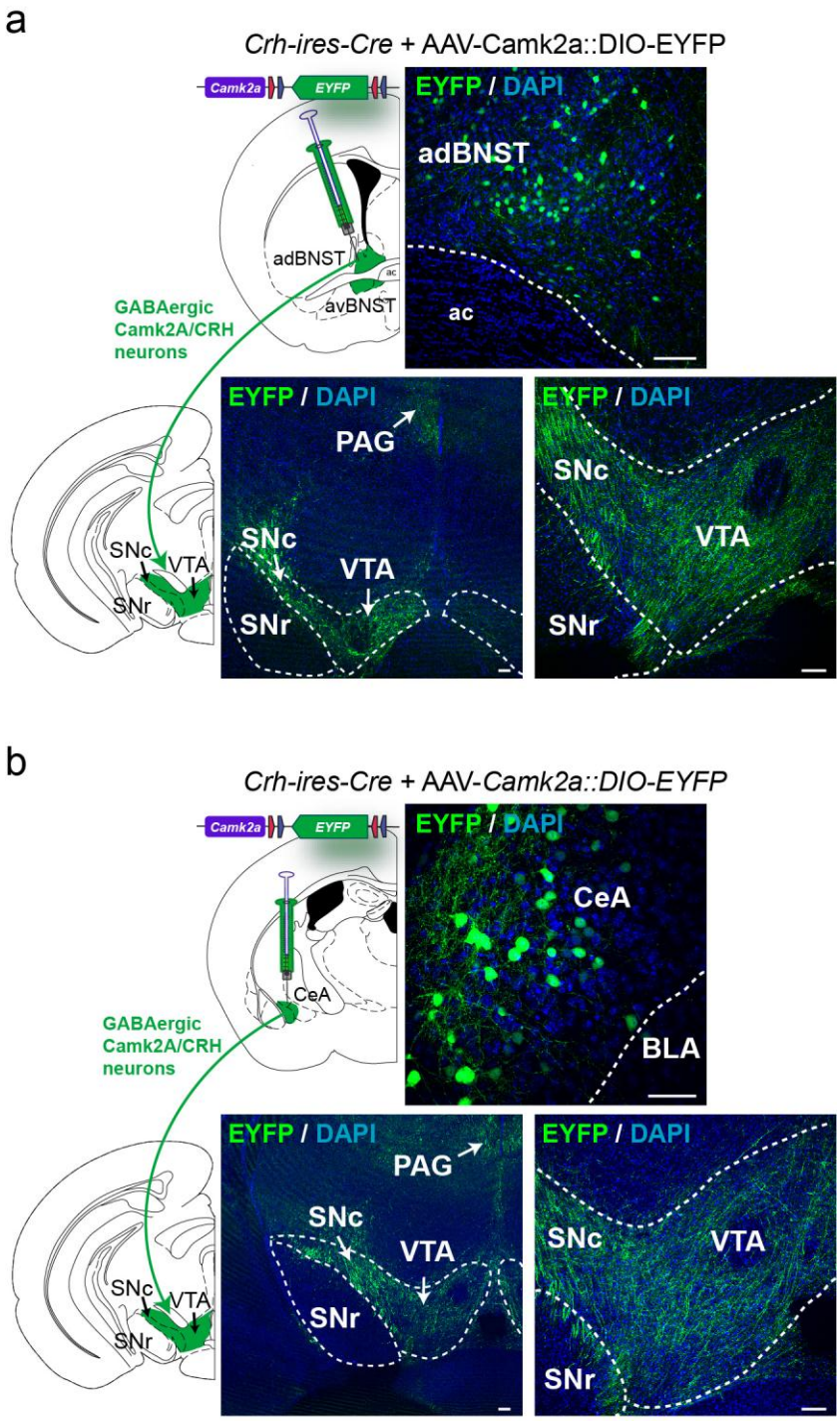

Supplementary Figure 6

CAMK2A-expressing CRH neurons in the aBNST and CeA project to the VTA.

Representative confocal images of *Crh-ires-Cre* mice injected with AAV-Camk2a::DIO-EYFP into the aBNST (**a**) or CeA (**b**). EYFP expression is driven by the Camk2a promoter specifically in CRH neurons. EYFP-labeled projections that originate from CAMK2A-expressing neurons of the aBNST or CeA (top panels) are detected in

the VTA and SNc (bottom panels). Bottom right depict higher magnification images of the VTA/SN midbrain region. Representative images were derived from three independent experiments each. Abbreviations: anterior commissure (ac), anterior dorsal BNST (adBNST), basolateral amygdala (BLA), central amygdala (CeA), periaqueductal gray (PAG), substantia nigra compacta (SNc), substantia nigra reticularis (SNr), ventral tegmental area (VTA). Scale bars represent 100 µm.

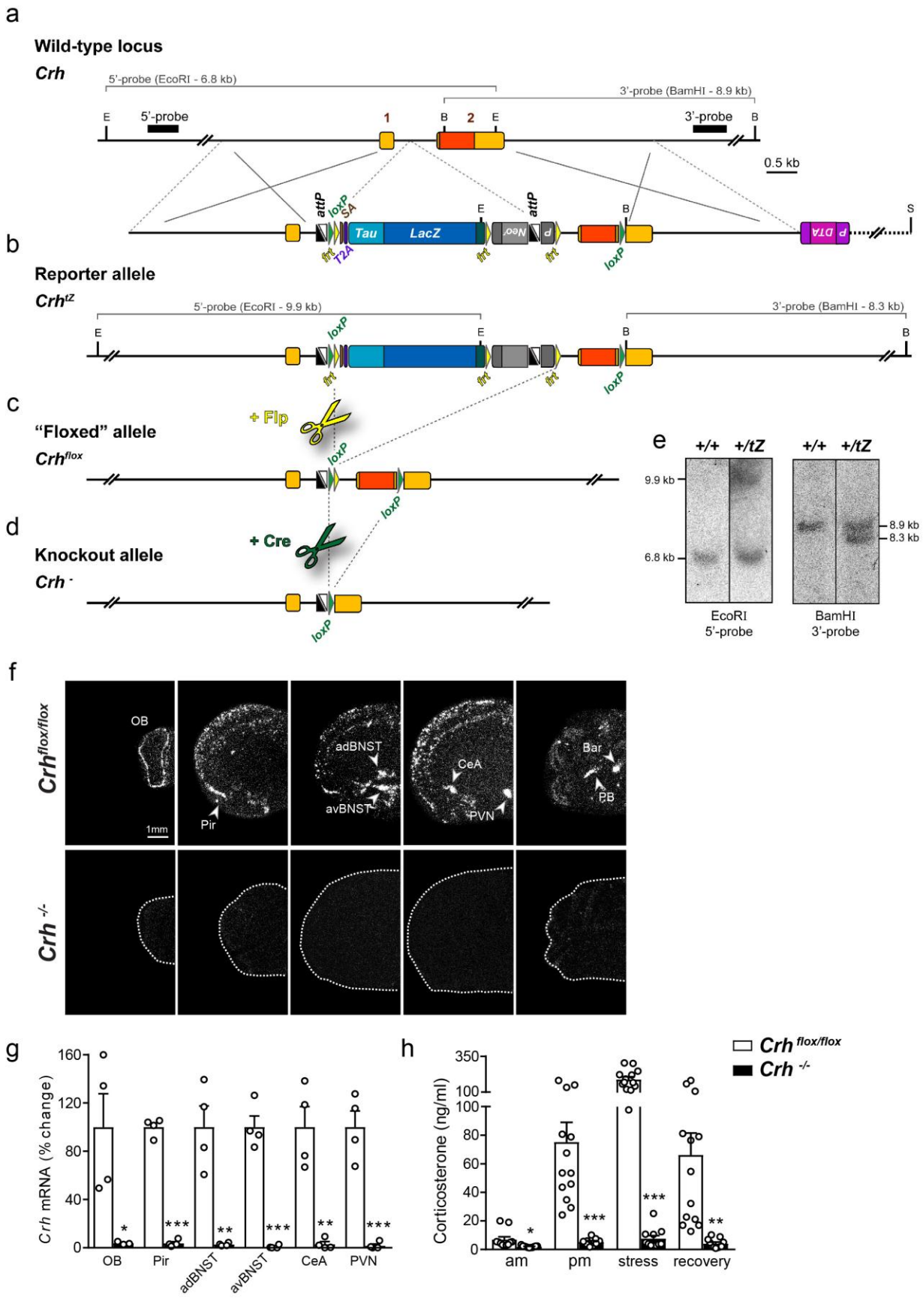
a
Wild-type locus
Crh
5'-probe (EcoRI - 6.8 kb)
3'-probe (BamHI - 8.9 kb)
E
5'-probe
1
B
2
E
3'-probe
B
0.5 kb
attP
loxP
SA
Tau
LacZ
E
attP
Neor
B
S
DTA
frt
T2A
frt
frt
loxP
b
Reporter allele
Crh tZ
5'-probe (EcoRI - 9.9 kb)
3'-probe (BamHI - 8.3 kb)
E
loxP
E
B
B
frt
frt
frt
loxP
c
+ Flp
"Floxed" allele
Crh flox
loxP
loxP
d
+ Cre
Knockout allele
Crh -
loxP
e
+/+
+/tZ
+/+
+/tZ
9.9 kb
6.8 kb
8.9 kb
8.3 kb
EcoRI
5'-probe
BamHI
3'-probe
f
Crh flox/flox
OB
1mm
Pir
adBNST
avBNST
CeA
PVN
Bar
PB
Crh -/-
g
Crh mRNA (% change)
160
120
80
40
0
OB
Pir
adBNST
avBNST
CeA
PVN
h
Crh flox/flox
Crh -/-
Corticosterone (ng/ml)
350
100
100
80
60
40
20
0
am
pm
stress
recovery

Supplementary Figure 7

Generation of conditional *Crh* knockout mice.

Strategy for targeted manipulation of the *Crh* locus. (**a**) Partial restriction maps of the wild-type locus and targeting vector. For better visualization, *loxP*, *frt* and *attP* sites are not to scale. (**b**) Recombined reporter allele (Crh^{tz}) following homologous recombination in embryonic stem (ES) cells. (**c**) Recombined floxed allele (Crh^{flox}) following removal of the *frt*-flanked reporter-selection cassette, and (**d**) conditional knockout allele (Crh^{-}) following Cre-mediated excision of the *loxP*-flanked exon 2. (**e**) Southern blot analysis of wild-type (+/+) and targeted ES cell clones (+/*tZ*). The external *Crh* 5'-probe was hybridized to *EcoRI*-digested genomic ES cell DNA. The targeted allele is indicated by the presence of an additional mutant (mt) 8.9 kb fragment. The *Crh* 3'-probe was hybridized to *BamHI*-digested DNA from the same ES cell clone confirming homologous recombination by detection of an additional mutant fragment at 8.3 kb. Homologous recombination was confirmed with two external probes in two independently prepared genomic DNA samples. (**f**) Functionality of the conditional *Crh* allele was confirmed by breeding Crh^{flox} mice to *Cre-Deleter* mice resulting in ubiquitous ablation of *Crh* mRNA expression throughout the brain determined by ISH (representative images from four independent experiments). (**g**) Quantification of *Crh* mRNA expression in (f), shown as percent change compared to littermate controls. Unpaired two-tailed t-test; OB ($t_{(6)}$ = 2.9, *p = 0.032); Pir ($t_{(6)}$ = 24.3, ***p < 0.0001); adBNST ($t_{(6)}$ = 5.6, **p = 0.0014); avBNST ($t_{(6)}$ = 10.7, ***p = 0.0013); CeA ($t_{(6)}$ = 5.7, **p = 0.0013); PVN ($t_{(6)}$ = 7.3, ***p = 0.0003); n = 4 mice/group, 1-2 sections/mouse). (**h**) Expectedly, ablation of CRH in $Crh^{-/-}$ mice also resulted in strongly diminished hypothalamic-pituitary-adrenal axis activity evident by significantly reduced corticosterone levels measured in the morning (am), evening (pm), and following 10 min (stress) and 90 min (recovery) of restraint stress. Unpaired two-tailed t-test - am ($t_{(20)}$ = 2.6, p = *0.017, n = 11 mice/group); pm ($t_{(20)}$ = 4.1, ***p = 0.0005, n = 13 $Crh^{flox/flox}$, 9 $Crh^{-/-}$); stress ($t_{(22)}$ = 8.9, ***p < 0.0001, n = 13 $Crh^{flox/flox}$, 11 $Crh^{-/-}$); recovery ($t_{(22)}$ = 3.7, **p = 0.0013, n = 13 $Crh^{flox/flox}$, 11 $Crh^{-/-}$). Error bars represent s.e.m.

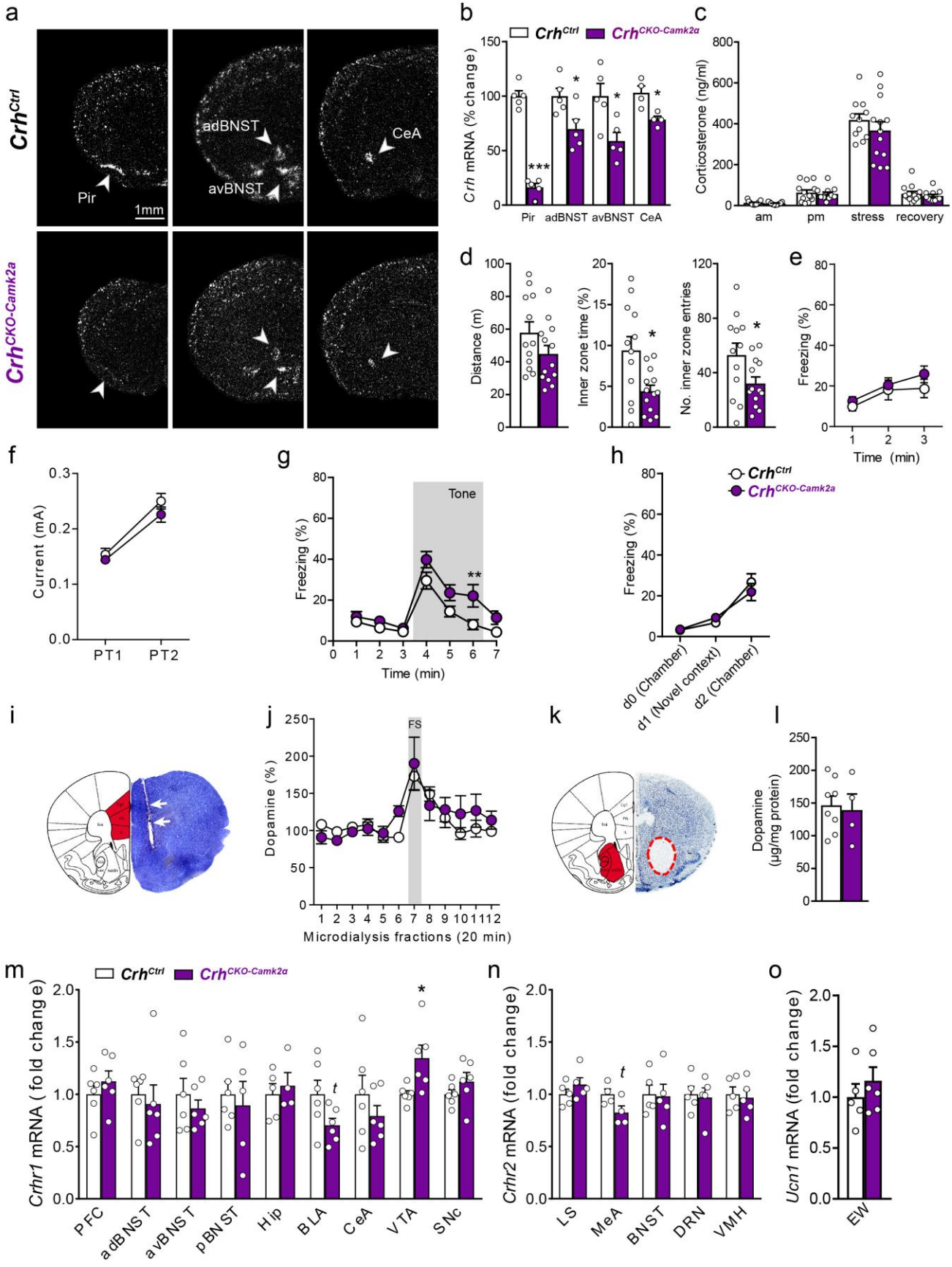
a
Crh^Ctrl
Crh^CKO-Camk2a
Pir
adBNST
avBNST
CeA
1mm
b
Crh^Ctrl
Crh^CKO-Camk2α
Crh mRNA (% change)
Pir
adBNST
avBNST
CeA
c
Corticosterone (ng/ml)
am
pm
stress
recovery
d
Distance (m)
Inner zone time (%)
No. inner zone entries
e
Freezing (%)
Time (min)
f
Current (mA)
PT1
PT2
g
Freezing (%)
Tone
Time (min)
h
Crh^Ctrl
Crh^CKO-Camk2a
Freezing (%)
d0 (Chamber)
d1 (Novel context)
d2 (Chamber)
i
j
Dopamine (%)
FS
Microdialysis fractions (20 min)
k
l
Dopamine (μg/mg protein)
m
Crh^Ctrl
Crh^CKO-Camk2α
Crhr1 mRNA (fold change)
PFC
adBNST
avBNST
pBNST
Hip
BLA
CeA
VTA
SNc
n
Crhr2 mRNA (fold change)
LS
MeA
BNST
DRN
VMH
o
Ucn1 mRNA (fold change)
EW

Supplementary Figure 8

Additional molecular and behavioral assessment of *Crh*$^{CKO\text{-}Camk2a}$ mice.

(**a**) Overview images and quantification (**b**) of *Crh* mRNA expression assessed by ISH in control and *Crh*$^{CKO\text{-}Camk2a}$ mice. Regions of interest are marked with arrowheads. Deletion of *Crh* in *Crh*$^{CKO\text{-}Camk2a}$ mice was primarily detected in the piriform cortex (Pir), and in a subset of neurons within the BNST and CeA. Thus, the deletion pattern in *Crh*$^{CKO\text{-}Camk2a}$ mice supports the expression maps obtained with double ISH (Supplementary Fig. 3). Unpaired two-tailed t-test; Pir ($t_{(8)}$ = 13.8, ****p < 0.0001); adBNST ($t_{(8)}$ = 2.7, *p = 0.028); avBNST ($t_{(8)}$ = 3.0, *p = 0.018); CeA ($t_{(8)}$ = 3.3, *p = 0.01); for Pir, adBNST and avBNST n = 5 mice/group, 1-2 sections/mouse; for CeA n = 4 mice/group, 1-2 sections/mouse. (**c**) Hypothalamic-pituitary-adrenal (HPA) axis activity was similar between control and *Crh*$^{CKO\text{-}Camk2a}$ mice, evident by comparable corticosterone levels measured in the morning (am), evening (pm), and following 10 min (stress) and 90 min (recovery) of restraint stress. Unpaired two-tailed t-test; am ($t_{(22)}$ = 1.1, p = 0.3, n = 13 *Crh*^{Ctrl}, 11 *Crh*$^{CKO\text{-}Camk2a}$); pm ($t_{(23)}$ = 0.45, p = 0.7, n = 13 *Crh*^{Ctrl}, 12 *Crh*$^{CKO\text{-}Camk2a}$); stress ($t_{(22)}$ = 0.95, p = 0.35, n = 11 *Crh*^{Ctrl}, 13 *Crh*$^{CKO\text{-}Camk2a}$), recovery ($t_{(22)}$ = 0.8, p = 0.43, n = 13 *Crh*^{Ctrl}, 11 *Crh*$^{CKO\text{-}Camk2a}$). (**d**) *Crh*$^{CKO\text{-}Camk2a}$ mice showed increased anxiety in the open field test (unpaired two-tailed t-test / inner zone time: $t_{(23)}$ = 2.8, *p = 0.01 / number of inner zone entries: $t_{(23)}$ = 2.1, *p = 0.044), without exhibiting changes in locomotion (unpaired two-tailed t test / distance travelled: $t_{(23)}$ = 1.6, p = 0.13; n = 12 *Crh*^{Ctrl}, 13 *Crh*$^{CKO\text{-}Camk2a}$). (**e**) Freezing time was similar between *Crh*$^{CKO\text{-}Camk2a}$ and control mice following contextual fear conditioning (RM ANOVA - time genotype x interaction: $F_{(2,52)}$ = 0.63, p = 0.54; n = 13 *Crh*^{Ctrl}, 15 *Crh*$^{CKO\text{-}Camk2a}$). (**f**) Foot shock perception, tested in a new cohort of mice, was not different between *Crh*$^{CKO\text{-}Camk2a}$ mice and littermate controls. Both, control and *Crh*$^{CKO\text{-}Camk2a}$ mice showed first signs of discomfort (backwards moving; PT1) and pain (jumping and vocalization; PT2) at similar foot shock current intensities (RM ANOVA - genotype: $F_{(1,21)}$ = 1.91, p = 0.18; genotype x current intensity: $F_{1,21}$ = 0.46, p = 0.505; n = 11 *Crh*^{Ctrl}, 12 *Crh*$^{CKO\text{-}Camk2a}$). This was also the case if only PT2 was considered (*Crh*^{Ctrl}: 0.26 ± 0.01 mA; *Crh*$^{CKO\text{-}Camk2a}$: 0.23 ± 0.01 mA; unpaired two-tailed t-test: t_{22} = 1.5, p = 0.15). (**g**) *Crh*$^{CKO\text{-}Camk2a}$ mice display higher levels of sensitized fear. After termination of PT2 in (f), all mice received an unsignalled foot shock (1.5 mA for 2s). The next day all animals were placed into a neutral context for a 3 min baseline period followed by a 3 min tone presentation. This procedure allows for the measurement of non-associative memory components of the conditioning procedure[39,42-45]. *Crh*$^{CKO\text{-}Camk2a}$ mice showed similarly low levels of freezing before and after tone presentation. However, *Crh*$^{CKO\text{-}Camk2a}$ mice displayed a sustained freezing response in particular towards the end of the (unconditioned) tone presentation (RM ANOVA - time: $F_{(6,132)}$ = 44.31, **p < 0.0001; Genotype: $F_{(1,22)}$ = 4.93, *p = 0.037; Genotype x Time: $F_{(6,132)}$ = 2.33, *p = 0.036; Bonferroni post-hoc test, *p < 0.05; n = 12 *Crh*^{Ctrl}, 12 *Crh*$^{CKO\text{-}Camk2a}$) suggesting impairments in fear adaptation. (**h**) *Crh*$^{CKO\text{-}Camk2a}$ mice show no changes in generalization of contextual fear. Compared to the freezing levels in the shock context before shock presentation on day 0, and to the novel context before tone presentation on day 1, both groups showed a

significantly higher freezing response upon re-exposure to the shock context on day 2. This validates the results in (e) and demonstrates again similar levels of contextual fear between control and *Crh*$^{CKO\text{-}Camk2a}$ mice (RM ANOVA - context: $F_{(2,22)} = 41.06$, ***$p < 0.0001$; Genotype: $F_{(1,22)} = 0.085$, $p = 0.773$; context x genotype interaction: $F_{(2,22)} = 1.18$, $p = 0.32$; n = 12 *Crh*^{Ctrl}, 12 *Crh*$^{CKO\text{-}Camk2a}$). (**i**) Representative coronal brain section (right) and corresponding atlas images (left) depicting the correct placement of microdialysis probes within the prefrontal cortex. (**j**) In vivo microdialysis showing a similar magnitude in footshock-induced dopamine release between control and *Crh*$^{CKO\text{-}Camk2a}$ mice (dopamine levels normalized to baseline levels (fractions 1-6) and depicted in percent) / RM ANOVA - genotype x time interaction $F_{(11,187)} = 0.89$, $p = 0.55$; genotype $F_{(1,17)} = 1.18$, $p = 0.29$; time $F_{(11,187)} = 7.06$, ***$p < 0.0001$; n = 10 *Crh*^{Ctrl}, 9 *Crh*$^{CKO\text{-}Camk2a}$. (**k**) Representative coronal brain section (right) and corresponding atlas images (left) depicting the micropunched area of the nucleus accumbens. (**l**) Basal dopamine tissue content in the nucleus accumbens was similar between control and *Crh*$^{CKO\text{-}Camk2a}$ mice (unpaired two-tailed t-test; $t_{(10)} = 0.28$, $p = 0.79$; n = 4 *Crh*^{Ctrl}, 8 *Crh*$^{CKO\text{-}Camk2a}$). (**m-o**) mRNA expression of *Ucn1*, *Crhr1* (determined by real-time qPCR; unpaired two tailed t-test; VTA $t_{(10)} = 2.28$, *$p = 0.046$; BLA $t_{(10)} = 2.0$, $p = 0.075$; PFC, adBNST, avBNST, BLA, CeA, VTA and SNc n = 6 mice/group; pBNST n = 6 *Crh*^{Ctrl}, 5 *Crh*$^{CKO\text{-}Camk2a}$; Hip n = 5 *Crh*^{Ctrl}, 4 *Crh*$^{CKO\text{-}Camk2a}$) and *Crhr2* (determined by ISH; unpaired two tailed t test; MeA $t_{(6)} = 2.1$, $p = 0.076$;n = 4 *Crh*^{Ctrl}, 4 *Crh*$^{CKO\text{-}Camk2a}$; LS, BNST, DRn and VMH n = 5 *Crh*^{Ctrl}, 5 *Crh*$^{CKO\text{-}Camk2a}$) across different brain regions. . Error bars represent s.e.m.

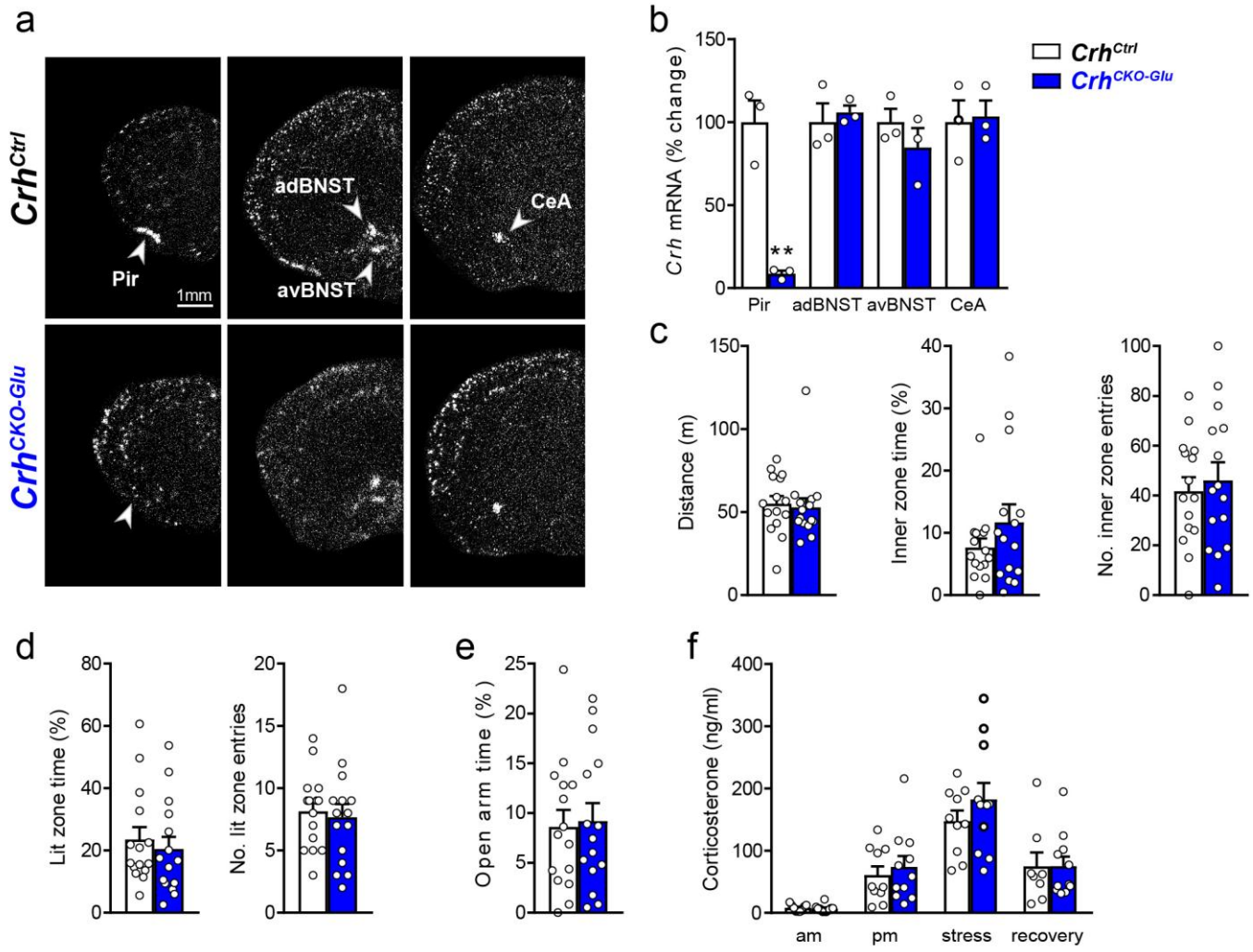

Supplementary Figure 9

Behavioral effects in *Crh*$^{CKO\text{-}Camk2a}$ mice are independent of *Crh* deletion in glutamatergic neurons.

Crh deletion specifically in glutamatergic neurons (*Crh*$^{CKO\text{-}Glu}$) was achieved by crossing *Crh*^{flox} mice with *Nex-Cre* mice. Overview images (**a**) and quantification (**b**) of *Crh* mRNA expression assessed by ISH in control and *Crh*$^{CKO\text{-}Glu}$ mice. Unpaired two-tailed t-test; Pir ($t_{(4)}$ = 6.9, **p = 0.002); adBNST ($t_{(4)}$ = 0.5, p = 0.65); avBNST ($t_{(4)}$ = 1.1, p = 0.34); CeA ($t_{(4)}$ = 0.21, p = 0.84); n = 3 mice/group, 1-2 sections/mouse. Deletion of *Crh* in *Crh*$^{CKO\text{-}Glu}$ mice was primarily detected in the piriform cortex (Pir, arrow, bottom panel) and a few single neurons in cortical layers II/III and V/VI (not visible in the overview images). Thus, the deletion pattern in *Crh*$^{CKO\text{-}Glu}$ mice supports the expression maps obtained with double ISH (Supplementary Fig. 3) and further confirms the absence of glutamatergic CRH neurons in the aBNST and CeA. (**c-e**) Locomotion (unpaired two-tailed t-test; $t_{(28)}$ = 0.29, p = 0.77), and anxiety-related behavior in the open field (unpaired two-tailed t-test; inner zone time (%): $t_{(28)}$ = 1.3, p = 0.22 / no. inner zone entries: $t_{(28)}$ = 0.48, p = 0.64), as well as anxiety-related behavior in the dark-light box test (unpaired two-tailed t-test; lit zone time (%): $t_{(28)}$ = 0.54, p = 0.59 / no.

lit zone entries: $t_{(28)} = 0.35$, $p = 0.72$) and EPM (unpaired two-tailed t-test; $t_{(28)} = 0.23$, $p = 0.82$) were not altered in $Crh^{CKO\text{-}Glu}$ mice compared to littermate controls; n = 15 mice/group. (**f**) HPA axis activity was similar between control and $Crh^{CKO\text{-}Glu}$ mice, evident by comparable corticosterone levels measured in the morning (am), evening (pm), and following 10 min (stress) and 90 min (recovery) of restraint stress. Unpaired two-tailed t-test / am ($t_{(19)} = 0.58$, $p = 0.57$; n = 9 Crh^{Ctrl}, 12 $Crh^{CKO\text{-}Glu}$) / pm ($t_{(19)} = 0.57$, $p = 0.58$; n = 10 Crh^{Ctrl}, 11 $Crh^{CKO\text{-}Glu}$) / stress ($t_{(19)} = 1.1$, $p = 0.3$; n = 10 Crh^{Ctrl}, 11 $Crh^{CKO\text{-}Glu}$) / recovery ($t_{(18)} = 0.76$, $p = 0.46$; n = 9 Crh^{Ctrl}, 11 $Crh^{CKO\text{-}Glu}$). Error bars represent s.e.m.

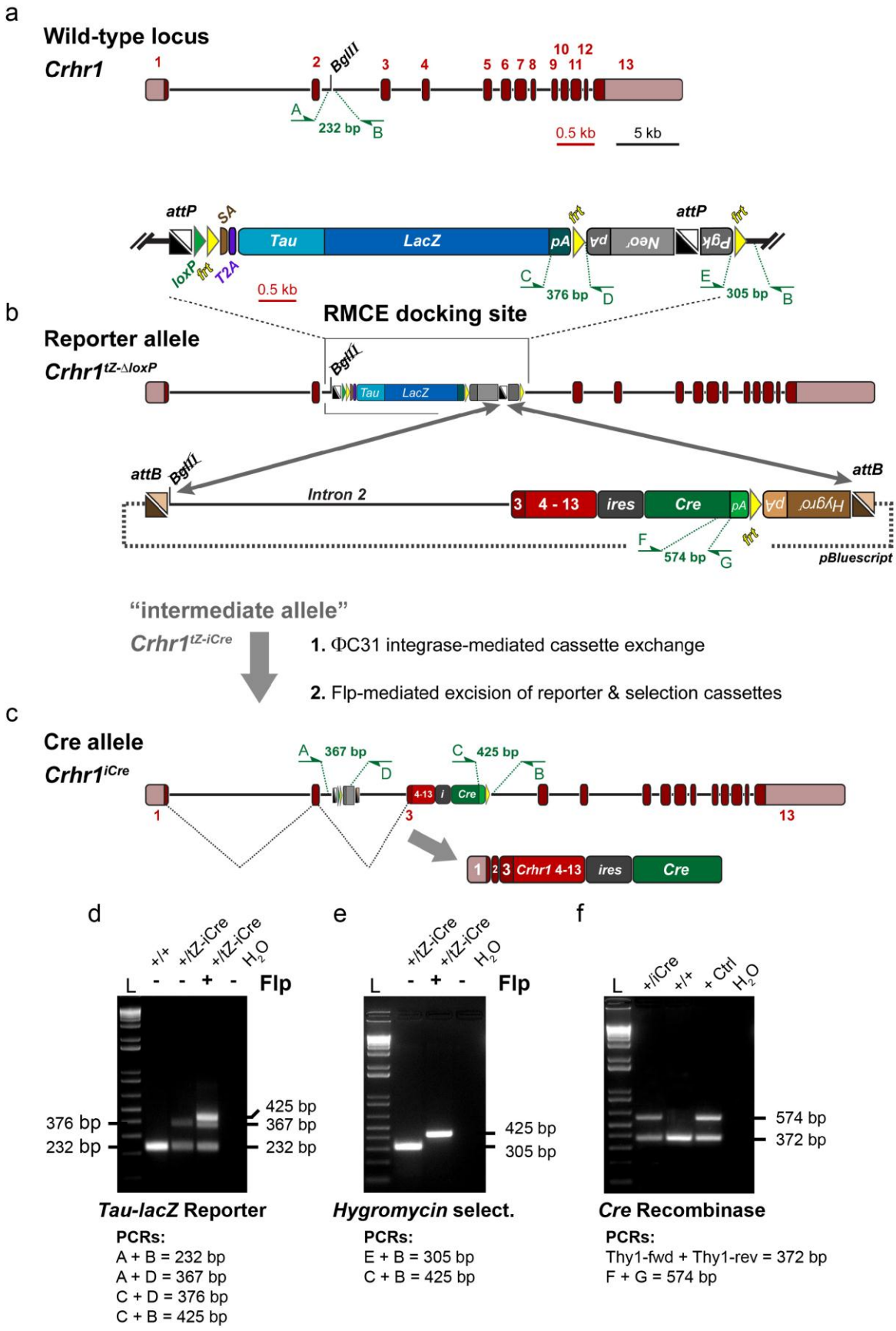
a
Wild-type locus
Crhr1
1
2
BglII
3
4
5 6 7 8
9 11
10 12
13
A
232 bp
B
0.5 kb
5 kb
attP
SA
Tau
LacZ
pA
Neo'
Pgk
attP
frt
loxP
frt
T2A
0.5 kb
C
376 bp
D
E
305 bp
B
b
RMCE docking site
Reporter allele
Crhr1tZ-ΔloxP
BglII
Tau
LacZ
attB
BglII
Intron 2
3
4 - 13
ires
Cre
pA
Hygro'
attB
F
574 bp
G
frt
pBluescript
"intermediate allele"
Crhr1tZ-iCre
1. ΦC31 integrase-mediated cassette exchange
2. Flp-mediated excision of reporter & selection cassettes
c
Cre allele
Crhr1iCre
A
367 bp
D
C
425 bp
B
4-13
i
Cre
1
3
13
1
2
3
Crhr1 4-13
ires
Cre
d
+/+
+/tZ-iCre
+/tZ-iCre
H2O
L
-
-
+
-
Flp
376 bp
232 bp
425 bp
367 bp
232 bp
Tau-lacZ Reporter
PCRs:
A + B = 232 bp
A + D = 367 bp
C + D = 376 bp
C + B = 425 bp
e
+/tZ-iCre
+/tZ-iCre
H2O
L
-
+
-
Flp
425 bp
305 bp
Hygromycin select.
PCRs:
E + B = 305 bp
C + B = 425 bp
f
+/iCre
+/+
+ Ctrl
H2O
L
574 bp
372 bp
Cre Recombinase
PCRs:
Thy1-fwd + Thy1-rev = 372 bp
F + G = 574 bp

Supplementary Figure 10

Generation of *Crhr1-ires-Cre* mice.

Strategy for targeted manipulation of the *Crhr1* locus. (**a**) Wild-type *Crhr1* locus depicting the position of integration of the docking site for recombinase-mediated cassette exchange (RMCE) in Intron 2. For better visualization different scales were used for exons and introns to illustrate the *Crhr1* gene structure. (**b**) *Crhr1*$^{tZ\text{-}\Delta loxP}$ allele containing the RMCE docking site in intron 2. A magnification of the docking site is provided above the *Crhr1*$^{tZ\text{-}\Delta loxP}$ allele. The targeting vector for RMCE equipped with respective *attB* sites is depicted below. Of note, *loxP*, *frt*, *attB*, *attP,* and *T2A* sites are not to scale. (**c**) ΦC31-mediated cassette exchange in embryonic stem (ES) cells resulted in integration of the targeting vector into the right *attP* site. ES cells were used to generate mice, which were subsequently bred to *FLPeR* mice to simultaneously remove the reporter and selection cassettes. (**c**) The correct integration and removal of selection and reporter cassettes was verified by PCR. (**d**) Detection of Flp recombinase-mediated removal of *Tau-lacZ* reporter cassette with PCR. (**e**) Confirmation of simultaneous Flp recombinase-mediated removal of the hygromycin selection cassette. (**f**) Detection of Cre recombinase expression cassette in *Crhr1* locus. PCRs in d-f were independently replicated in each individual animal (within the respective mouse line) that was genotyped (n > 20).

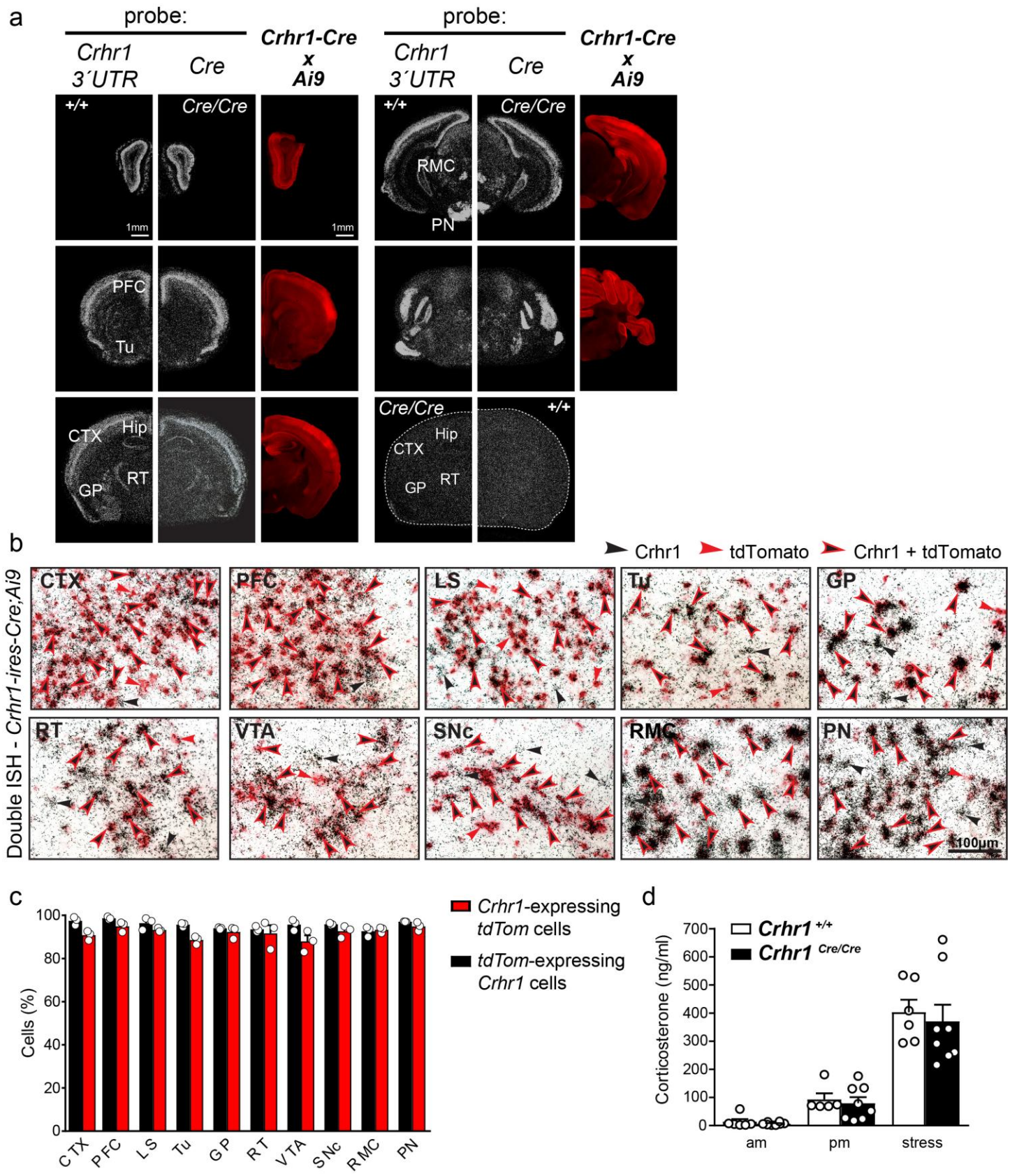

Supplementary Figure 11

Validation of *Cre* expression and recombination specificity in *Crhr1-ires-Cre* mice.

(**a**) *Cre* mRNA expression fully recapitulates the endogenous *Crhr1* mRNA expression pattern. The first row depicts endogenous *Crhr1* mRNA expression in *Crhr1*$^{+/+}$ mice (rostral to caudal), determined by ISH using a radiolabeled riboprobe detecting the *Crhr1* 3'UTR which is not expressed from the *Crhr1-ires-Cre* allele. The second row shows a similar hybridization signal in *Crhr1*$^{Cre/Cre}$ littermates, using a *Cre*-specific riboprobe. Riboprobe specificity and targeting accuracy is further illustrated by the absence of a *Crhr1* 3'UTR signal in *Crhr1*$^{Cre/Cre}$ mice (see targeting approach in Supplementary Figure 10), and absence of a *Cre* signal in their wildtype littermates. The third row shows representative images of *Crhr1*$^{Cre/Cre}$ mice crossed with *Ai9* reporter mice (R26::*loxP-STOP-loxP-tdTomato*). tdTomato fluorescence (red staining) mirrors the native *Crhr1* expression pattern (silver grains). Images are representatives from three independent experiments. (**b**) High specificity of Cre recombinase expression in CRHR1 neurons was additionally confirmed by double ISHs against endogenous *Crhr1* (silver grains) and *Crhr1-ires-Cre*-driven *tdTomato* (red). Images are representatives from three independent experiments. (**c**) Quantification of double positive cells in (b); n = 3 mice from independent experiments, 1-2 sections/mouse. Most tdTomato-expressing neurons co-expressed *Crhr1,* and likewise the majority of *Crhr1*-positive neurons also expressed *tdTomato* (red-framed, black arrowheads). Upon Cre recombinase-mediated removal of the transcriptional STOP cassette from the R26CAG::*loxP-STOP-loxP-tdTomato* allele, *tdTomato*-reporter expression is driven by a CAG promoter and continuously detected in all neurons that have expressed CRHR1 at any given time point within their lineage. Thus, *tdTomato*-positive neurons that lack *Crhr1* expression (red arrowheads) could represent cells that expressed CRHR1 during the course of development, but ceased to do so in adulthood. The presence of *Crhr1*-positive, but *tdTomato*-negative cells (black arrowheads), could be explained by lack of activity of the CAG promoter (that drives *tdTomato* expression) in those particular cells. **(d)** HPA axis activity was similar between *Crhr1*$^{+/+}$ and *Crhr1*$^{Cre/Cre}$ mice, evident by comparable corticosterone levels measured in the morning (am), evening (pm), and following 10 min of restraint stress (stress). Thus, in addition to its expression, functionality of CRHR1 activity is not compromised in *Crhr1*$^{Cre/Cre}$ mice (unpaired two-tailed t-test: am $t_{(12)}$ = 0.86, p = 0.41; n = 6 *Crhr1*$^{+/+}$, 8 *Crhr1*$^{Cre/Cre}$ / pm $t_{(11)}$ = 0.41, p = 0.69; n = 5 *Crhr1*$^{+/+}$, 8 *Crhr1*$^{Cre/Cre}$ / stress $t_{(12)}$ = 0.42, p = 0.68; n = 6 *Crhr1*$^{+/+}$, 8 *Crhr1*$^{Cre/Cre}$). Abbreviations: cortex (Ctx), globus pallidus (GP), hippocampus (Hip), lateral septum (LS), pontine nuclei (PN), prefrontal cortex (PFC), reticular thalamic nucleus, red nucleus (RMC), substantia nigra, pars compacta (SNc), olfactory tubercle (Tu), ventral tegmental area (VTA). Error bars represent s.e.m.

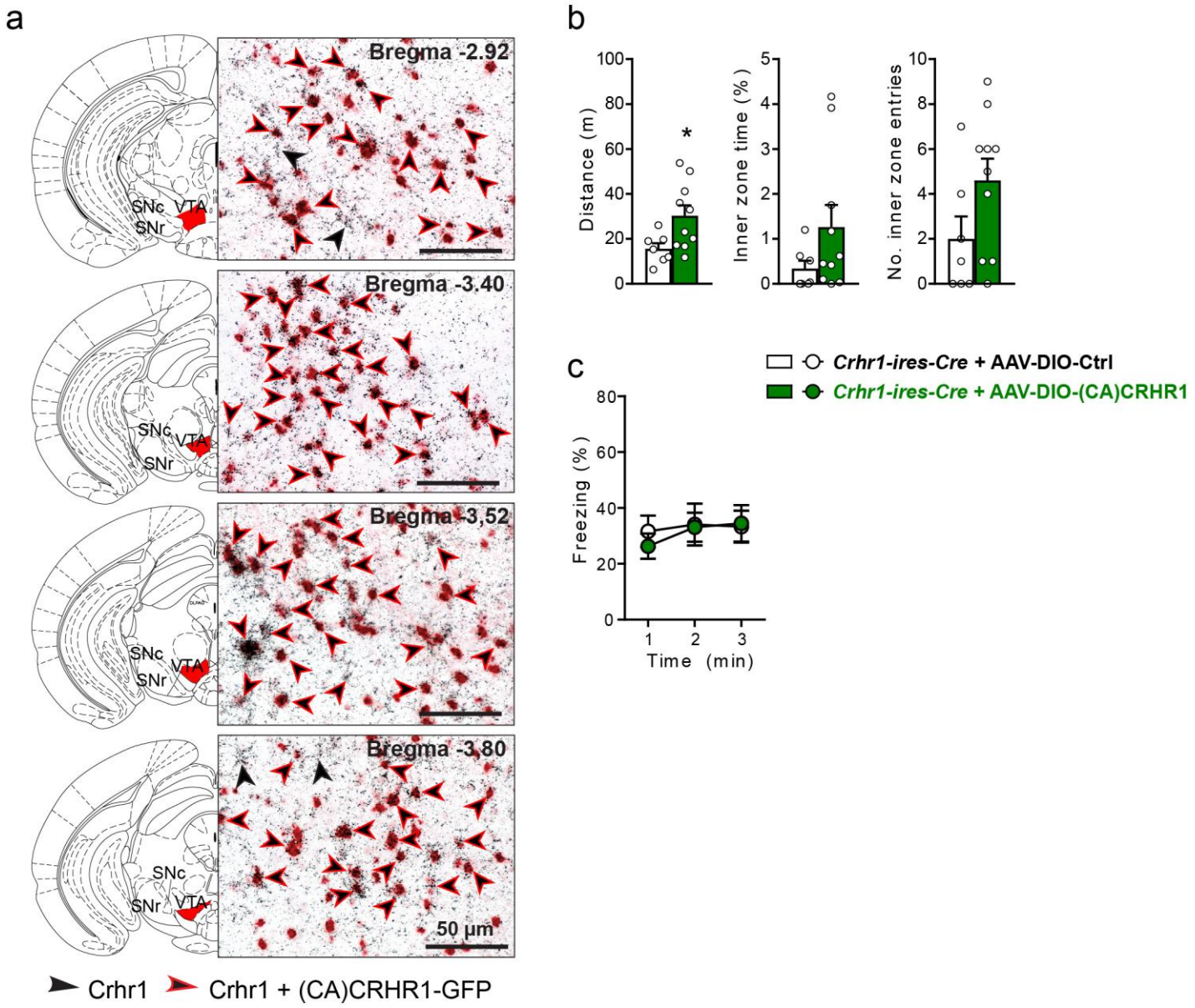

Supplementary Figure 12

Virally mediated expression of a constitutively active (CA) CRHR1-EGFP fusion construct in VTA neurons of *Crhr1-ires-Cre* mice.

(a) Double ISH against GFP (red staining) and endogenous *Crhr1* (silver grains) in *Crhr1-ires-Cre* mice following VTA-injection of AAV-Ef1α::(CA)CRHR1-GFP (representative coronal sections are shown from rostral to caudal; corresponding atlas images are shown on the left). The vast majority of cells co-express GFP and native *Crhr1* (red-framed black arrow), further demonstrating recombination-specificity of the *Crhr1-Cre* driver. Images are representatives from three independent experiments. **(b)** *Crhr1-ires-Cre* mice expressing (CA)CRHR1-EGFP in the VTA exhibit increased locomotion in the OF (unpaired two-tailed t-test: $t_{(15)} = 2.45$, *p = 0.027*), and a trend towards decreased anxiety compared to controls injected with AAV-Ef1α::DIO-mCherry

(unpaired two-tailed t-test: inner zone time (%) - $t_{(15)} = 1.5$, $p = 0.15$; no. inner zone entries - $t_{(15)} = 1.8$, $p = 0.09$; n = 8 *Ctrl*, 10 *(CA)CRHR1)*. Although locomotion in the open field was increased it is unlikely to compromise the interpretation of the other tests (Fig. 3) given that mice expressing CA(CRHR1) also displayed reduced anxiety in the marble burying task (Fig. 3l), an assay in which confounding increases in locomotion would have produced the opposite effect. **(c)** No changes between groups were observed during contextual fear conditioning (RM ANOVA – time x genotype interaction: $F_{(2,34)} = 0.45$, $p = 0.64$; genotype: $F_{(1,17)} = 0.05$, $p = 0.82$; n = 8 *Ctrl*, 11 *(CA)CRHR1*). Error bars represent s.e.m.

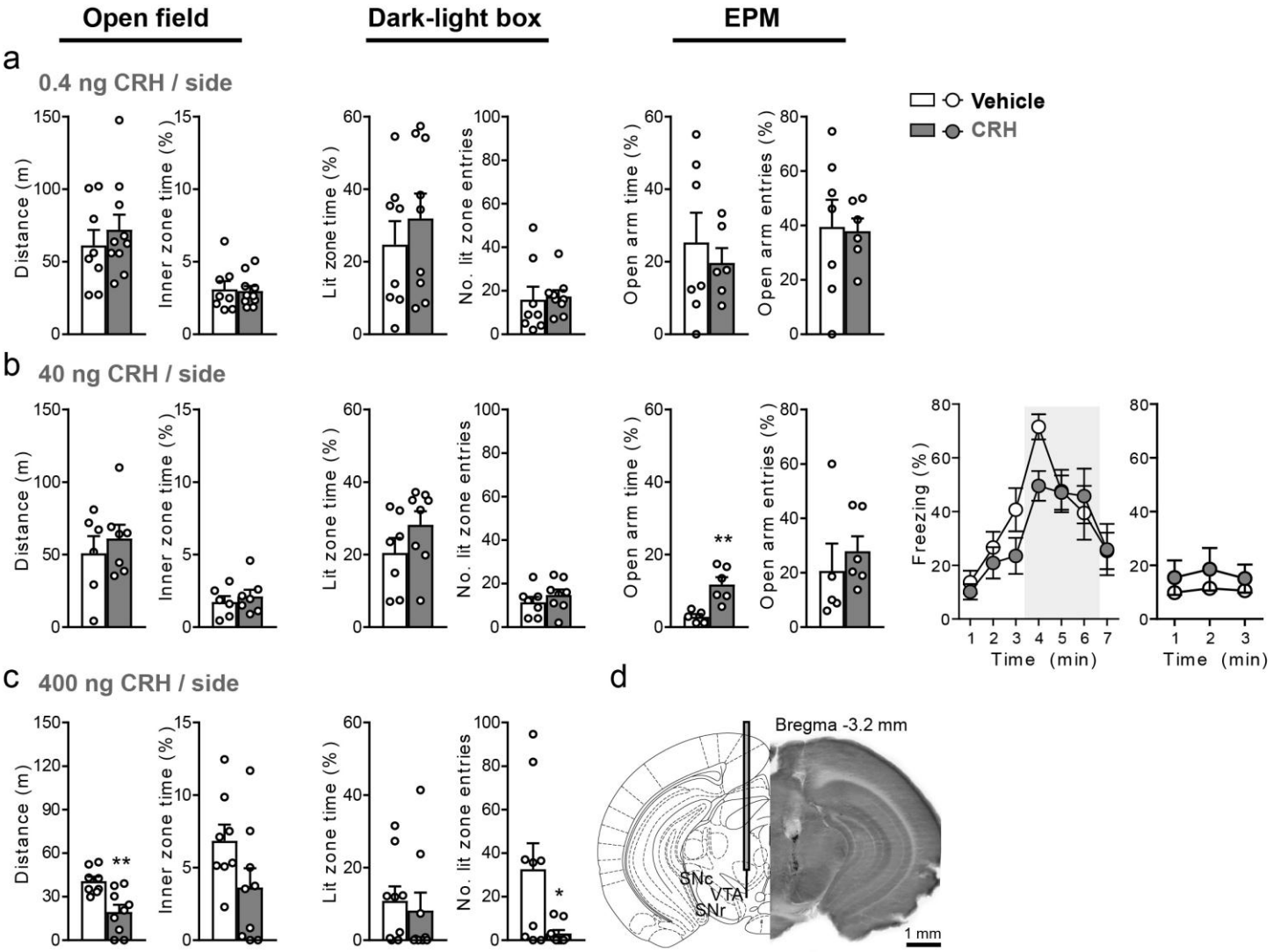

Supplementary Figure 13

CRH microinjections into the VTA decrease anxiety at specific doses.

Bilateral injections of CRH into the VTA of wildtype C57BL/6J mice at **(a)** 0.4, **(b)** 40 and **(c)** 400 ng/side. No behavioral alterations were observed at the lowest CRH dose (unpaired two-tailed t-test / OF: distance $t_{(16)}$ = 0.71, p = 0.49; inner zone time (%) $t_{(16)}$ = 0.18, p = 0.86; n = 8 Vehicle, 10 CRH / DaLi: lit zone time (%) $t_{(15)}$ = 0.75, p = 0.46; no. lit zone entries $t_{(15)}$ = 0.23, p = 0.82; n = 8 vehicle, 9 CRH / EPM: open arm time (%) $t_{(11)}$ = 0.58, p = 0.57; open arm entries (%) $t_{(11)}$ = 0.14, p = 0.89; n = 7 vehicle, 6 CRH). Microinjections of 40 ng/side induced decreased anxiety-related behavior specifically in the EPM (unpaired two-tailed t-test: $t_{(9)}$ = 3.95, **p = 0.003, n = 5 vehicle, 6 CRH) without alerting locomotion or cued fear conditioning (unpaired two-tailed t-test / OF: distance $t_{(11)}$ = 0.52, p = 0.66; inner zone time (%) $t_{(11)}$ = 0.60, p = 0.56; n = 6 vehicle, 7 CRH / DaLi: lit zone time (%) $t_{(13)}$ = 1.4, p = 0.19; no. lit zone entries $t_{(13)}$ = 0.93, p = 0.37; n = 7 vehicle, 8 CRH / EPM: open arm entries (%) $t_{(11)}$ = 0.66, p = 0.53; n = 5 vehicle, 6 CRH / fear conditioning (RM ANOVA) – tone/auditory:

time x genotype interaction $F_{6,72} = 1.83$, $p = 0.11$; genotype $F_{1,12} = 0.42$, $p = 0.69$ / context: time x genotype interaction $F_{2,24} = 0.53$, $p = 0.59$; genotype $F_{1,12} = 0.40$, $p = 0.75$; n = 7 vehicle, 7 CRH). At the highest dose of 400 ng/side, CRH induced a pronounced decrease in locomotion in the OF (unpaired two-tailed t-test / OF: distance - $t_{(15)} = 3.5$, **p = 0.003; inner zone time (%) $t_{(15)} = 1.83$, $p = 0.09$; n = 8 vehicle, 9 CRH) and lead to a decrease in number of lit zone entries in the DaLi (unpaired two-tailed t-test / DaLi: lit zone time (%) $t_{(16)} = 0.43$, $p = 0.67$; no. lit zone entries $t_{(16)} = 2.5$, *p = 0.025; n = 9 vehicle, 9 CRH). **(d)** Representative coronal brain section (right) and corresponding atlas image (left) depicting the correct placement of the injection cannula in the VTA. Error bars represent s.e.m.

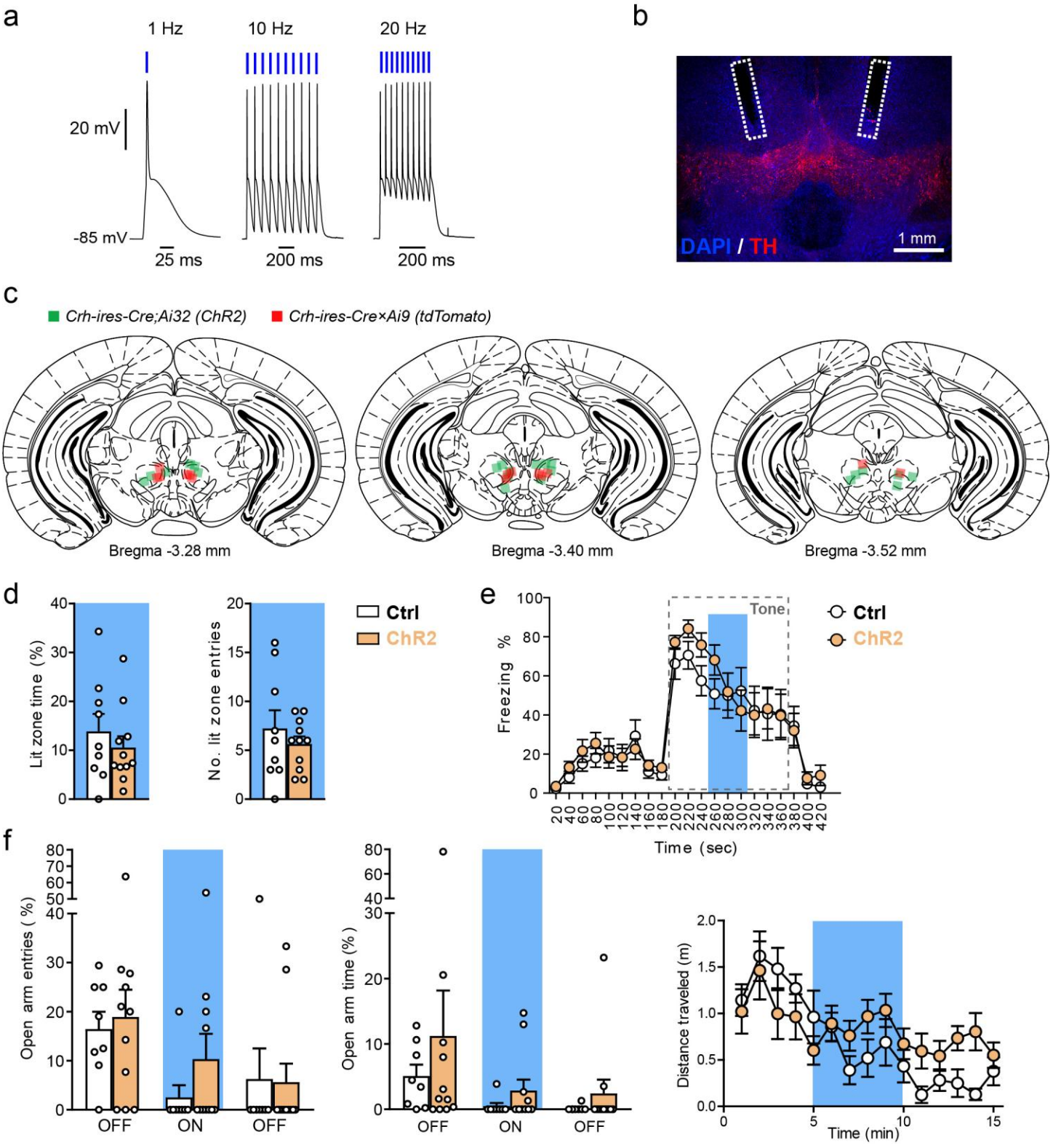

Supplementary Figure 14

Acute optogenetic activation of VTA-targeting CRH terminals does not alter anxiety.

Optogenetic activation of CRH-positive terminals within the VTA was performed in *Crh-ires-Cre* mice bred to ChR2-expressing Ai32 mice. This enabled targeting of all VTA-projecting CRH fibers without having to perform multiple viral injections and optic fiber placements in the BNST and CeA. Lack of local CRH-expressing cell bodies in the VTA ensured the predominant activation of VTA-targeting CRH fibers. **(a)** Electrophysiological confirmation of optogenetic activation of a subset of ChR2-expressing CRH neurons of the CeA in acute brain slices. Current-clamp recordings show that ChR2-expressing CRH neurons fire an action potential to single blue laser pulses (488 nm, 2 msec, 5 mW/mm², 1 Hz) and can follow 10 Hz and 20 Hz laser stimulation (representative of n = 4 animals). **(b)** Representative coronal image showing the optic fiber tract (white dashed line) above the VTA. **(c)** Individual, bilateral placements of optic fiber tips in the VTA of *Crh-ires-Cre* mice bred to ChR2-expressing Ai32 animals (green) and *Crhr-ires-Cre* mice bred to Ai9 reporter mice (red). **(d-f)** VTA-targeting CRH fibers were stimulated by delivering blue (460 nm) light (20 Hz, 15 ms pulses) via bilateral optical fibers implanted over the VTA.. **(d)** Photostimulation of VTA-projecting CRH fibers in the ChR2 group did not affect anxiety in the DaLi (light ON during the entire test) or **(e)** cued fear conditioning (1 min light epoch shown in blue) compared to tdTom-expressing controls (unpaired two-tailed t-test for DaLi – lit zone time (%) $t_{(18)} = 0.82$, $p = 0.43$; no. lit zone entries $t_{(18)} = 0.84$, $p = 0.41$; n = 9 Ctrl, 11 ChR2 / RM ANOVA for FC – genotype x time interaction $F_{(20,340)} = 0.75$, $p = 0.78$; genotype $F_{(1,17)} = 0.30$, $p = 0.59$; n = 8 Ctrl, 11 ChR2). **(f)** 15 min session in the EPM with alternating OFF-ON-OFF illumination epochs (5 min each). No significant effect of light stimulation was detected in ChR2 mice for open arm entries or open arm time (RM ANOVA / open arm time (%): group x epoch interaction $F_{(2,34)} = 0.22$, $p = 0.81$; group $F_{(1,17)} = 1.1$, $p = 0.31$; epoch $F_{(2,34)} = 2.7$, $p = 0.08$: open arm entries (%): group x epoch interaction $F_{(2,34)} = 0.5$, $p = 0.61$; group $F_{(1,17)} = 0.45$, $p = 0.51$; epoch $F_{(2,34)} = 4.7$, $^{*}p = 0.014$; n = 8 Ctrl, 11 ChR2). Both, Ctrl and CrhR2 mice appeared to exhibit time-dependent habituation to the EPM, as seen by a gradual decrease in distance travelled/exploration already during the first 5 min (RM ANOVA: group x time interaction $F_{(14, 238)} = 2.2$, $^{**}p = 0.008$; genotype $F_{(1,17)} = 0.7$, $p = 0.42$; time $F_{(14,238)} = 8.7$, $^{***}p < 0.0001$; n = 8 Ctrl, 11 ChR2). Error bars represent s.e.m.

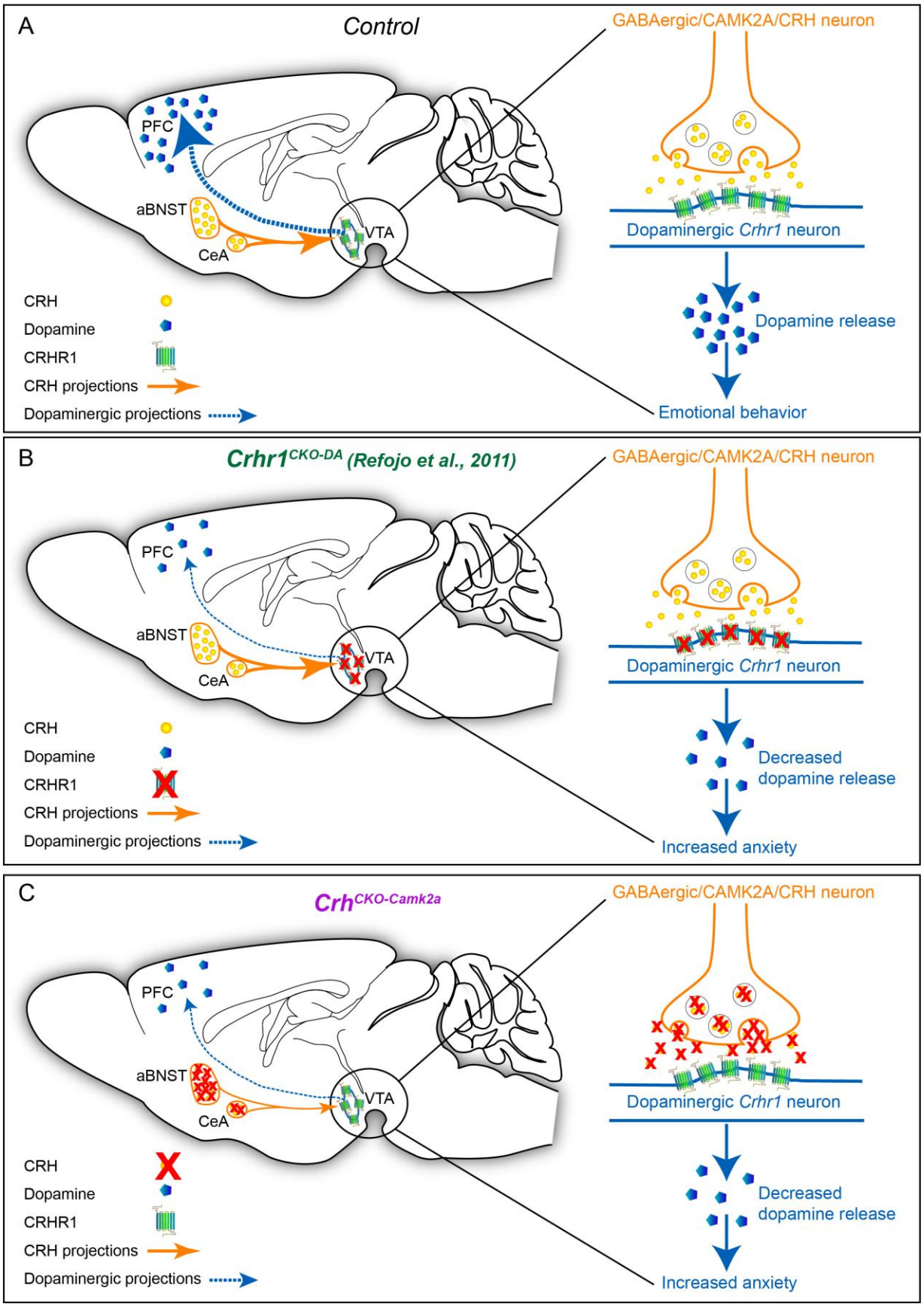
A
Control
GABAergic/CAMK2A/CRH neuron
PFC
aBNST
CeA
VTA
Dopaminergic Crhr1 neuron
Dopamine release
Emotional behavior
CRH
Dopamine
CRHR1
CRH projections
Dopaminergic projections
B
Crhr1CKO-DA (Refojo et al., 2011)
GABAergic/CAMK2A/CRH neuron
PFC
aBNST
CeA
VTA
Dopaminergic Crhr1 neuron
Decreased dopamine release
Increased anxiety
CRH
Dopamine
CRHR1
CRH projections
Dopaminergic projections
C
CrhCKO-Camk2a
GABAergic/CAMK2A/CRH neuron
PFC
aBNST
CeA
VTA
Dopaminergic Crhr1 neuron
Decreased dopamine release
Increased anxiety
CRH
Dopamine
CRHR1
CRH projections
Dopaminergic projections

Supplementary Figure 15

Working model of the anxiolytic CRH circuit.

(**a**) In control mice under baseline conditions, GABAergic/CAMK2A/CRH neurons in the anterior bed nucleus of the stria terminalis (aBNST) and central amygdala (CeA) project monosynaptically to the ventral tegmental area (VTA). There, presynaptic CRH release activates postsynaptic CRHR1 on VTA-to-prefrontal cortex (PFC) projecting (mesocortical) dopaminergic neurons to modulate dopamine release, and thereby alter anxiety. (**b**) Conditional deletion of *Crhr1* in dopaminergic neurons (*Crhr1*$^{CKO\text{-}DA}$ mice) results in diminished dopamine release in the PFC and increased anxiety behavior[1]. Similar effects are observed when *Crh* is deleted from VTA-targeting GABAergic/CAMK2A/CRH neurons in the aBNST and CeA (*Crhr1*$^{CKO\text{-}Camk2\alpha}$ mice).

Supplementary Table 1. Projection areas of CRH neurons in the anterior bed nucleus of the stria terminalis (aBNST), central amygdala (CeA), paraventricular nucleus of hypothalamus (PVN), piriform cortex (Pir) and prefrontal cortex (PFC). Most prominent projection targets of CRH neurons across different brain regions are listed based on the intensity of the synaptophysin-GFP (Syp-GFP) staining. Ratings range from week (+) to very strong (++++) Syp-GFP puncta density. The highest density of VTA-innervating CRH terminals originated in the aBNST and CeA. GABAergic CRH neurons in the PFC mainly projected locally. Glutamatergic CRH neurons in the Pir did not innervate the VTA. Data from three independent experiments. Abbreviations: basolateral amygdala (BLA), dorsal raphe nucleus (DRN), lateral amygdala (LA), medial amygdala (MeA), periaqueductal gray (PAG), substantia nigra (SN), ventral tegmental area (VTA).

aBNST		CeA		PVN		Pir		PFC	
Brain region	**SYP density**	**Brain region**	**SYP density**	**Brain region**	**SYP density**	**Brain region**	**SYP density**	**Brain region**	**SYP density**
aBNST (dorsal & ventral)	++++	aBNST (dorsal & ventral)	+++	NAc core	+	Pir	+++	Prelimbic cortex	+++
Posterior BNST	+++	Ventral palidum	++	BNST	++	Claustrum	+++	Infralimbic cortex	+++
Thalamic nuclei	++	Dorsomedial hypothalamus	+	Thalamic nuclei	++	Accessory olfactory bulb	++	Cingulate cortex	+++
Hypothalamic nuclei	+++	MeA	++	BLA and LA	++	Lateral hypothalamus (peduncular part)	++		
MeA	+++	PAG	++	Hypothalamic nuclei	+++				
PAG	++	DRN	++	PAG	+++				
DRN	++	VTA	++	Median eminence	++++				
VTA	+++	SNc	+++	VTA	+				
SNc	+								